
Article:
Mahdi, FM orcid.org/0000-0002-3046-4389, Mehrabi, M, Hassanpour, A orcid.org/0000-0002-7756-1506 et al. (1 more author) (2019) On the formation of core-shell granules in batch high shear granulators at two scales. Powder Technology, 356. pp. 253-262. ISSN 0032-5910

https://doi.org/10.1016/j.powtec.2019.08.019

On the Formation of Core-Shell Granules in Batch High Shear Granulators at Two Scales

Mahdi F.M., Mehrabi M., Hassanpour A. and Muller F.L.*

School of Chemical and Process, Engineering, University of Leeds, LS2 9JT, UK

*E-mail address of corresponding author: F.L.Muller@leeds.ac.uk

Abstract

High shear granulation of powders with a wide size distribution can lead to the formation of core-shell particles consisting of a few larger particles in the core with a shell of fine particles. We demonstrate successful scale down of core-shell granule formation and, using a new model for interpreting observed cross-sections, show that above a critical speed the shell-thickness remains constant at about ~5% of the granule diameter with a crushing strength of about 5.5MPa. Below this speed and at low fill-levels, shell-thickness increases and granule strength reduces. Under a low mixing intensity at the lowest fill-levels core-shell particles are not formed at all.

Theoretical work on the strength of liquid bridges shows that small particles attached to each other would redistribute more easily than the same particles attached to a large particle. We propose therefore that a detachment-reattachment process is responsible for the formation of core-shell granules.

Keywords: High shear wet granulation, Core-shell granules, Seeded granulation, Liquid bridges and Shell thickness determination

1 Introduction

Granulation is an important process widely used and applied for the aggregation of powder clusters in various industries including mineral processing, agricultural products, detergents, pharmaceuticals, food, and specialty chemicals. This technique has been used for improving the macroscopic and microscopic structures, flowability and handling of material, bulk density, and products appearance as well as reducing the dust formation of products and pressure loss for fluid flow through a packed bed [1-5].

A number of researchers have extensively studied the granulation of calcium carbonate powder using different binders and granulator types. For example, polyethylene glycol (PEG 4000) as a binder and Zanchetta Roto Junior granulator (10 L) have been used by [6-11]. Furthermore, Kristensen and Hansen [12] have used Glatt GPCG-1.1 granulator (2 L) and polyvinyl povidone (PVP) as a binder. In addition, there is a significant amount of research on wet granulation available in the literature [8, 13-15]. Generally, the findings are more concentrated on fundamental understanding of granulation process, granule size and surface appearance of the granules than internal structure characterisation of the produced granules.

Rahmanian et al. [16-18] and Antony et al. [19] observed that powders with a wide size distribution can be granulated in such a manner that core-shell type granules consisting of large particles in the centre surrounded by a layer of agglomerated fines can be formed through a process termed as “seeded granulation”. It was observed that these core-shell granules have narrower distributions of granule size, uniform, structure, higher strength and density resulting in improved flowability and reduced bulk density. Rahmanian and co-workers [16-19] granulated calcium carbonate (Durcal 65) with aqueous polyethylene glycol (PEG4000) as binder in a Cyclomix high-shear mixer granulator with different scales (1, 5, 50 and 250 L) and varying impeller tip speed, fill level and binder addition rate. Furthermore, three scale-up rules: constant impeller tip speed, constant shear stress and constant Froude number were used. They

found that, at constant impeller tip speed conditions, the core-shell granules were produced at all four scales (1, 5, 50 and 250 L) of the granulator. Production of core-shell type granules was reported to be a function of the feed particle size distribution and the operating conditions of the granulator. It was observed that operating the Cyclomix granulator at impeller tip speeds lower than 3.5 m/s (regardless of the scale) reduced the yield of core-shell granules within the desired granule size range. Therefore, the constant impeller tip speed rule was proposed for scale up [16].

In addition, to study the effect of the feed's particle size distribution on the production of core-shell granules, three grades of calcium carbonate powder, namely Durcal 15, 40 and 65 were analysed by Rahmanian et al. [16]. Their study showed that Durcal 65 powder contained more coarse particles (above 120 μm) with sufficiently wide particle size distribution for formation of about 95-100% core-shell granules within the desired particle size range (500 to 600 μm). Furthermore, it was found that the optimal percentage of liquid/solid for producing more core-shelled was about 10%. When the percentage of binder increases, the trends shift towards formation of coarse granules [5, 20]. One of the main questions which yet to be answered is whether the formation of core-shell granules can be replicated in other granulators with different geometries and scales. Hence, this work evaluates the granulation of Durcal 65 in a different high shear granulator, focusing on smaller scales, and more in-depth analysis of the mechanisms of core-shell granule formation.

2 Materials and methodology

2.1 Materials

Calcium carbonate powder (Durcal 65, Omya UK Ltd) and aqueous polyethylene glycol (pluriol E4000 powder, BASF) as a binder were used for the granulation process. Table 1 shows the properties of both materials. The SEM images in Fig 1 show the morphology of the calcium

carbonate powder (Durcal 65) a cubical particle. The size distribution of the calcium carbonate powder (Durcal 65) was obtained by two methods: Malvern 2000 (dry system) and sieve analysis, as shown in Fig 2. In the sieve analysis, a 300 g sample was used with a series of 10 ASTM standard sieves vibrated for 30 min in a Haver sieves shaker (EML 200 premium, H&B Wire Fabrications LTD, Germany). The Micromeritics Tristar 3000 was used to measure the BET surface area (m^2/g) for the materials. While the density of solids was found using Micromeritics Acupyc 1330. Furthermore, mean aspect ratio, circularity and elongation were measured using the Malvern Morphologi G3S. The Scanning Electron Microscope (HITACHI Benchtop TM3030 Plus) was used to analysis the samples images.

2.2 Granulation methodology

In this work, a small scale, top driven and batch high-shear wet granulator (MiPro, ProCepT, Zelzate, Belgium) was used, as shown in Fig 3. Experiments were conducted in two geometrically similar granulator vessels of different scales: 0.5 and 1.9 L. The agitator torque was recorded continuously. The high-speed chopper within the granulator was not used during this study.

The same methodology followed was as discussed in [1, 16, 18, 21]. The binder solution, 65 wt% solution of PEG 4000, was prepared by dissolving the PEG 4000 powder in reverse osmosis water (RO-Water) at temperature of 60°C while stirring to ensure complete dissolution. The solution was cooled down to at least 30°C before use. A measured quantity of Durcal 65 powder was added into the granulator bowl and sealed off. The granulator was turned on for an initial stage of 20s with the calculated impeller tip speed using Eq. (1) [4, 22] to prevent any segregation and ensure that the particle bed is homogeneous. Then, 10 wt% (with respect to the Durcal mass) of the PEG 4000 binder solution, was added to the powder bed all at once (all the binder in one shot) through a top manhole. This is based on Rahmanian et al [18] and Hassanpour et al. [1] investigations. The granulation then continued up to the process

time as calculated using Eq. (2) [4]. For different cases and conditions, these are shown in Table 2.

$$\frac{N_x}{N_y} = \left(\frac{D_y}{D_x}\right)^n \qquad \text{Eq. (1)}$$

$$\frac{t_x}{t_y} \propto \left(\frac{S_y}{S_x}\right)\left(\frac{V_x}{V_y}\right) \qquad \text{Eq. (2)}$$

In the equations above N, D, t, S and V are the impeller tip speed (m/s), the impeller diameter (m), the process time (s), the granulator bowl surface area (m^2) and the volume of feed material (L), respectively. Furthermore, x and y are the required and the reference information, respectively and n is a constant according to the impeller tip speed (n=1.0, in this case). The reference point was used from Hassanpour data [1] for 5L case. On completion of the procedure the agitator is stopped, and the final product dried at 30℃ for 12 h.

The different conditions and scales used are summarised in Table 2: two different scales (0.5 and 1.9 L) with three different batch volumes: 25%, 50% and 75% of the bowl volume. Each batch volume was tested at four different impeller tip speeds (3.50, 4.13, 5.39 and 6.12 m/s) and the run using 4.13 rpm was repeated four times to test repeatability and reliability of the data. A total of 42 experiments have been conducted and analysed in this work.

2.3 Granule analysis

Sieving was carried out to characterise the dried granules for size distribution. A complete batch sample from 90 to 1000 g (dependant on the batch volume) was sieved using a series of 12 ASTM standard sieves. A Haver sieves shaker (EML 200 premium, H&B Wire Fabrications

LTD, Germany) was used for 10 min per run. The amplitude and period were set as 1.0 mm and 8 s, respectively to minimise breakage of granules as discussed by Rahmanian et al [23].

Granules in the size range of 500–600 μm, were selected for the strength and structure analysis, so as to allow comparison to the results from other authors [2, 19, 20, 24]. The arithmetic mean diameter (d_w) on a weight basis for each sample was calculated as explained by other authors [25, 26].

The crushing strength of the granules was analysed using the Instron 5566 Universal Testing Machine. Granules are compressed between two rigid plates until a sudden drop in the applied load detects their breakage. For each granulation run, 30 randomly selected granules were tested with a maximum load of 10 N and a loading velocity of 0.083 mm/s. More details on the test procedure and the method are given by number of authors [27-29]. The nominal crushing strength, σ (Pa) is equal to the crushing load, F (N) divided by the cross sectional area, $A = {\pi}/{4}\, D^2$ (m^2) of the granule (using the averaged diameter for the 500-600 μm sieve fraction):

$$\sigma = \frac{F}{A} \qquad \text{Eq. (3)}$$

The crushing strength of a granulation run is described by the average and standard deviation of the 30 tests.

2.4 Structure visualisation

In preparation for the core structure analysis of granule, the sampled granules were embedded in resin. A 30 mm mould with removable base was filled with 1-2 mm depth of sample. The resins used are epoxides: EpoThin and Araldite, which are two-component resins (resin and hardener). EpoThin mix ratio is 1:0.45 g resin to hardener (HY 951). Araldite (DBF) mix ratio is 10:1 by volume resin/ hardener. About 12- 15 mm depth of resin was poured into each mould and left for overnight to dry. Initially, P600 silicon carbide grinding papers were used with the

solid blocks to reveal sample across its face. After that, P1200 grit paper was used to refine the surface. The block was polished using a 6 μm diamond paste (Struers Monocrystalline) for 5-6 min. This step was repeated using finer diamond pastes: 3, 1 and 0.25 μm. In addition, to prevent "plucking" in the samples, fluid is not used within this process. The structure of the granules was analysed using a Scanning Electron Microscope (HITACHI Benchtop TM3030 Plus).

A number of SEM images for each sample was taken. Then, a manual thresholding method using AVIZO software was applied to identify particles. After that, using the naked eye the granules with a visible core were counted. A particle was considered to have a core if the one or more large particles where completely surrounded by significantly smaller particles. The core-shell fraction (f_{cs}, yield %) is the ratio of the granules with a visible core to the total number of granules detected.

3 Results and discussion

3.1 Impeller torque

The recorded impeller torque profile was used as a guide to monitor the granulation process stages, as shown in Fig 4. The net torque value was found by subtracting the empty machine torque (no material) from the total recorded torque (with materials). Fig 4 shows five values of the net torque based on the stages of granulation process in this work. Stage (1) shows the net torque for the mixing of solid particles without any liquid. Stages (2) and (3) show the maximum and minimum net torque respectively just after adding the liquid binder. Once the binder is well distributed, Stages (4) and (5) show the average and the final net torque, respectively. This experiment was run four times for all fill levels, confirming the reproducibility of the granulation process.

3.2 Granules size

Fig 5 shows the size distribution (D10, D50 and D90) of granules obtained at different batch volume (0.125, 0.250, 0.375, 0.500, 1.00 and 1.50 L) and impeller tip speeds (3.50, 4.13, 5.39 and 6.12 m/s). In all cases, granule sizes are an order of magnitude larger than the Durcal 65 starting material. Error bars at 4.13 m/s represent the standard deviations of four runs for each experiment, again demonstrating an excellent reproducibility.

The granule size appears to be increasing with batch volume, but the trend is weak, and is more apparent the 1.9L bowl size. For example, increasing the batch size from 0.50 to 1.5 L in 1.9 L bowl at 6.12 m/s, increases the D50 granule size from 300 to 400 μm and the D90 from 1000 to 2000 μm.

The granule size appears to be independent of agitator speed at the 0.5L bowl size. The D10 and D50 appear to be constant or increase slightly in the 1.9L bowl, the D90 in contrast reduces significantly as agitator speed increases. For example, at a batch size of 1.0 L, increasing the impeller tip speed from 3.50 to 6.12 m/s decreases the D90 from 2000 to 1000 μm. It appears that the force on the granules exceed their strength only in very specific circumstances, and it is not clear why the 0.5L scale does not respond to agitator speed.

3.3 Granule structure

Core Shell type granules where observed for most granulations executed. Fig 6 shows a typical example of granules and polished slice of SEMs for the size range of 500 to 600 μm. To assess the reproducibility four identical runs were completed using the 0.5 L and 1.9 L at all fill levels and 4.13 m/s impeller tip speed, as shown in Fig 7 (for 50% fill level). The mean particle size, strength were highly reproducible with low standard deviations. The final granule size distribution varied a little between scales but the repeats at one scale have a very low standard deviation (less than ±3.3%). The granule strength of the 500-600 μm sieve fraction differs

between scales by a factor of 2.0. The standard deviations of the strength data is ±0.18% and ±0.24% for the 0.25L (in small scale 0.5L) and 1.0L (in large scale 1.9L) respectively.

3.4 Core-shell formation process

An over view of the core-shell granulation process observations is schematically presented in Fig 8. According to Lister and Ennis [5, 30] the mechanism of granulation had three stages: (i) wetting, nucleation and binder distribution then (ii) consolidation and growth and finally (iii) attrition and breakage. This mechanism results in the random arrangement of particles at granule level.

Newitt and Conway [31] state that there are five different states of saturation of liquid-bound granules: pendular, funicular, capillary, droplet and pseudo-droplet. The capillary state occurs when a granule is fully saturated, while in the pendular state particles are held together by liquid bridges at their contact points. The funicular state is a transition between the pendular and capillary state (the voids are not fully saturated with liquid). The droplet state occurs when the particles are held within or at the surface of a liquid drop. It is also possible to have a pseudo-droplet state were unfilled voids remain trapped inside the droplet (likely to occur in poorly wetting systems).

Iveson et al. [3] observed that the nucleation mechanism is influenced by the relative sizes of the droplet to primary particle size. Building on this Schaefer and Mathiesen [32] proposed two different nucleation mechanisms for melt agglomeration (Fig 9 A and C) and this has been extended to use for wet granulation as well [11]. This model explains identifies two regimes (route A) droplets significantly larger than the initial particle size and (route C) droplets and particles of similar size. For route A, granule nucleation will occur by immersion of the smaller particles into the larger drop that leads to produce nuclei with saturated pores. For route C,

nucleation will occur by distribution of the drops on the surface of the particles, which will then start to coalesce. In this case, air might be trapped inside the nuclei [32].

In both routes (A) and (C) particles are held together by liquid bridges. The liquid bridges' static surface tension force between two, either unequal or equal-sized spherical particles as well as a sphere with flat plate has been studied by number of authors [3, 33-37]. They found that, the capillary force and the total adhesion force (F) between particles decrease with increasing the contact angle and the size ratio of smaller to larger particle, as shown in Eq (4) as function of the normalised liquid volume (V^*) as represented by Eq (5).

$$F^*\left(1+{}^{R_L}/_{R_S}\right)={}^{F}/_{\pi\gamma R_S} \qquad \text{Eq. (4)}$$

$$V^*=\frac{V_{Liquid}}{V_L+V_S} \qquad \text{Eq. (5)}$$

Where, F is the adhesion force and F^* the normalised force of adhesion (defined by Eq (4)), R_L and R_S are the radius of the large and small particles, respectively, γ is the surface tension of the bridging liquid, V^* is the normalised liquid volume and V_L and V_S are the volume of the large and small particles respectively. Mehrotra and Sastry [35] observed that the normalised adhesion force F^* between a large and a small particle becomes independent of the liquid volume between the two particles when $V^* < 10^{-4}$.

In Fig 10, we plot the $F^*\left(1+{}^{R_L}/_{R_S}\right)$ at V^*=1e-6 obtained from Fig 5 in ref [35] vs. R_S/R_L as this yields the dimensionless force ${}^{F}/_{\pi\gamma R_S}$ on the small particle. It can be observed that for a small particle of constant size, the dimensionless force increases as the particle it is attached to increases in size (R_S/R_L decreases). In the limit $R_S/R_L \to 0$ the large particle is a flat surface, to which the small particle attaches with a force that is 2.95/1.86=1.56 times as high as the attachment to an equal-sized particle.

The mechanism of core-shell granulation appears to be different from route A and C in Fig 9 the larger core particles are not randomly distributed within a granule. To understand the mechanism of core-shell granulation formation. Hassanpour et al. [38] studied the mechanism of core-shell granulation using the discrete element method (DEM) simulations. Their results show that during granulation the core-shell granules grow by adhesion and reduce in size by breaking under shear deformation. This gives rise to varied sizes and coordination numbers [38]. However, their simulation results are not in full agreement with the results obtained through experimental work by Rahmanian et al [16] at higher rotational speeds.

Based on our observation below, that in systems with a wide, or bimodal size distribution, at the right conditions most granules consist of a large core covered by a shell of fine particles. We propose route B in which the large particles interact with similar size droplets and wet. Small particles will attach to the surface of a large particle by the formation of a liquid bridge strong enough to absorb the momentum of the small particle during attachment. These smaller particles may subsequently detach due forces exerted during subsequent collisions. As demonstrated above, small particles nearer to the surface of a large particle are more strongly bound than small particles attached to other small particles, e.g. those “sticking out” tend to break off, and subsequently may re-attach in places where more or stronger bridges can form (e.g. in a gap where more of its surface is near surrounding particles). Two or more granules or large particles can aggregate to create a larger granule with multiple larger particles in its centre as shown near the end of Route B in Fig 9. The Detachment-Reattachment process will be highly dependent on the speed at which particles collide with either the agitator, or with each other, hence fill level, agitator speed and scale all affect the nature of the final core shell granule.

3.5 Shell thickness

The observations of the cross-section of granules, shows both granules with, and granules without core. Here we propose a boiled egg model to explain this observation. All eggs have a yolk but depending on where the egg is cut, the yoke may be visible, or not. Likewise, we assume all granules have a core, whether of the core of a granule is visible or not depends on the where the centre of a granule is with respect to the polished sample's surface. Fig 11 shows schematically a number of possible locations resulting in planes at different levels which then will reveal different internal structure of the same granule. For example, both planes A-A and E-E result in the granule for which the core cannot be observed, a so called 'noncore-*shell'* granule, because the polishing depth is not enough to reach the core crystal. However, the other planes will result in a cross section that will reveal the larger particles at the centre, resulting in 'core-*shell'* granules with different number of crystals: plane B-B shows one crystal, plane C-C shows two crystals and plane D-D shows three crystals. It follows, that if all granules are core-shell granules, the SEM of the 2D polished surface will show a number of particles with core, and a number without.

If the total number of granules in the cross sectional slice is n_{tot}, the number of granules observed to have a core is n_c, then the fraction of cut granules $f_{nc} = 1 - f_{cs}$ that do not appear to have a core is:

$$f_{nc} = 1 - \frac{n_c}{n_{tot}} \qquad \text{Eq. (6)}$$

Given the granule diameter d_p, core diameter D_c the shell thickness δ_s, follows from the assumption that the distance of the granule's centre to the polished surface is random. The fraction granules cut through the shell only will then be $2\delta_s/d_p$ (for spherical eggs that is!). This should equal the observed fraction of particles without core: f_{nc}. The shell thickness δ_s is then.

$$\delta_s = f_{nc}\frac{d_p}{2} \qquad \text{Eq. (7)}$$

The observed values of δ_s/d_p for granules in the size range 500-600 µm are in Figure 12 as function of impeller tip speed for a range of fill levels. Each value is the average of four cross sections slides. Error bars have been added to the plot, however, they are small and not visible (average StDev is ±0.05%). In this granulator type, increasing the impeller tip speed results in a lower fraction of granules without core, and thus a thinner shell. At ~ 5 m/s, a critical speed is exceeded causing the small particles to detach and reattach more easily, resulting in thinner shells (2 to 8%), and little sensitivity to agitation speed. The granules in SEM image 13A where produced above the critical speed. With granules subjected to high forces the de- and re-attachment process is active (route B) resulting in core-shell granules in line with observations of previous research using a 5L Cyclomix granulator by Rahmanian et al. [16].

Shell thickness increases at speeds below the critical speed, and is also affected by the fill level. Between 3 and 4 m/s, granules shell thickness δ_s/d_p increases as high as 15%. At the lowest fill level, in the 0.5L scale the number of detachment process essentially stops, and the granules are no longer core shell particles. Fig 13B shows that the internal structure of the granules contains larger particles at random locations and these are not a core-shell granules; the reattachment process (route B) is clearly not active.

3.6 Particle size distribution criterion for the formation of core shell particles

The minimum shell thickness is one layer of small particles, on a large core particle. The volume percentage of the core to the fine particle (shell) can be found from.

$$f_{v,core} = \frac{V_{core}}{V_{granule}} = \frac{\left(d_p\left(1-\frac{2\delta_s}{d_p}\right)\right)^3}{d_p^3} = \left(1-\frac{2\delta_s}{d_p}\right)^3 \qquad \text{Eq. (8)}$$

In order to generate granules with δ_s/d_p =10% shell thickness (Fig 12B), equivalent to 500-600 µm, the volume percentage of the shell is 27%. This corresponds well to the distribution of the Durcal 65 (Fig 2B), with 35% particles smaller than 40 µm, indicating multiple layers are formed. With granules of 500-600 µm large, we observe that the shell is indeed made up of fines smaller than 10% of the final granule size, and as can be seen in the SEMs (Fig 13A) these represent 1 – 3 layers of particles smaller than the layer thickness, with an average thickness of ~1.5 d_{fine}. The size distribution of the granules is broad (Fig 7) and many contain multiple larger particles. This suggest that the volume of small particles (d_{fine}<10% d_p) found in the shell must be large enough to cover the surface of the larger particles ($d_p > d_{large}$) in the feed material (which is consistent with Route B in Fig 9)

$$wt\%\left(d_p < d_{fine}\right) \approx wt\%\left(d_p \gg d_{fine}\right)\frac{6}{d_{large}} * 1.5 * d_{fine} \qquad \text{Eq. (9)}$$

With $6/d_{large}$ converting volume to area, and assuming the density is the same for all particles. Applying this criterion to the Durcal distribution (Fig 2) with 20% of particles are larger than 100mu (say 200 µm) a rough estimate of the wt fraction of fines that would leads to formation of core shell particles is $20\% \times 9 \times \frac{40}{200} = 36\%$. Note that many granules contain more than one large particles, and a significant fraction (~10%) of fine material is located in the core of the granules.

3.7 Granules strength characterisation

The crushing strength of granules is described by the average and standard deviation of thirty 500-600 μm granules picked at random (Fig 14). In general, the granules crushing strength lies between 2 and 9 MPa, which compares well to the value of 8 MPa obtained by Rahmanian et al. [24] at 1L scale. At constant agitator speed, the crushing strength increases with the batch volume (weight of material) increases and reaches an asymptotic value of 5-6MPa. This is more

pronounced at the lower agitator speeds where the asymptotic value is achieved only at the highest batch sizes. Above the critical speed where the shell thickness becomes constant, crushing strength is also essentially constant at 5.5 MPa, though at the lowest fill level this may still be a little lower. This is consistent with the granulation mechanism proposed earlier and agrees with the previous work of many authors [1, 23, 39, 40]. As explained by Rahmanian et al [41] higher impeller tip speeds cause intensive mixing and compaction of the granules to a high degree that leads to produce high granule strength and a uniform strength distribution.

We suggest in addition that at constant agitator speed higher fill levels result in denser particle beds which causes higher shear forces on the particles. As a result the smaller particles break off and redistribute resulting in lower shell thickness, and stronger agglomerates (route B in Fig 9)

4 Conclusion

The focus of the paper is on mechanistic understanding of the formation of core shell particles we postulate that the shell results from redistribution of fines as fines connected to large particles are more firmly attached then fines attached to other similar small particles. The granulation of Durcal 65 with a wide size distribution in a ProCepT MiPro granulate at 0.5L and 1.9L scale demonstrated successful scale down of the formation of core shell granules to laboratory scale. We found that the fine material essentially covers the surface of the larger particles in the feed resulting in core shell particles. We show that core shell granules are formed at small scale as long as the mixing intensity is such that fines at the surface of granules get redistributed. Hence with sufficient fill volume and agitation speed core shell granules can be formed at all scales. If the rate of fines redistribution is too low, softer agglomerates are formed, in which larger particles are randomly dispersed.

The MiPro granulator processes in a highly reproducible way as evidenced by the similarity of the torque profiles of repeat runs, and the high reproducibility of the granules particle size distribution (d50: 300-400 μm). The size distribution is practically independent of agitator speed. Only the D90 at the larger scale reduced with increasing agitation speed.

The nature of the core shell granules was observed using cross sections of granules in the range of 500-600 µm. This showed core-shell granules to consist of a core consisting of one or more large particles (d_p>100 µm) dispersed in a mixture of smaller material, surrounded by a shell of fine material (d_p<10 µm). Assuming all granules contained cores, but only a fraction of the cross sections would result in that core being displayed in a cross section (e.g. like cutting a boiled egg) allowed estimation of the average shell thickness (δ_s / d_p) of ~5% for tip speed above a critical speed of 4 to 5 m/s. Below this both speed and fill level affect the shell

thickness, with lower values the thickness increases up to ~15% after which the material essentially is no longer a core shell particle, but a loose agglomerate.

This is also reflected in the granule's crushing strength of particles. Above the critical speed the crushing strength is 5.5MPa and this reduces for lower speeds and fill levels.

Based on theoretical strength of liquid bridges, we propose a new granulation mechanism where small particles are more easily detached when connected to other small particles compared to small particles attached to large particles. The force on the small particles increases with agitator speed, as well as with fill level, and results in a larger extend of redistribution of the small particles resulting in denser, thinner shells. At the critical speed the strength of the liquid bridge of a small particle is readily overcome during collisions.

Granulation is an important unit operation for many sectors, and with up to 30% of material in the shell, the understanding of core shell granule formation presented here underpins engineering design of new structured materials for use in end user formulations.

Acknowledgements

This project has received funding from the European Union's Horizon 2020 research and innovation programme under grant agreement No 637232

References

[1] A. Hassanpour, C.C. Kwan, B.H. Ng, N. Rahmanian, Y.L. Ding, S.J. Antony, X.D. Jia, M. Ghadiri, Effect of granulation scale-up on the strength of granules, Special Issue: 3rd International Workshop on Granulation: Granulation across the Length Scales3rd International Workshop on Granulation across the Length Scales, 189 (2009) 304-312.

[2] M.A. Behjani, N. Rahmanian, N. Fardina bt Abdul Ghani, A. Hassanpour, An investigation on process of seeded granulation in a continuous drum granulator using DEM, Advanced Powder Technology, 28 (2017) 2456-2464.

[3] S.M. Iveson, J.D. Litster, K. Hapgood, B.J. Ennis, Nucleation, growth and breakage phenomena in agitated wet granulation processes: a review, Granulation and Coating of Fine Powders, 117 (2001) 3-39.

[4] D.M. Parikh, Handbook of Pharmaceutical Granulation Technology, Third Edition, CRC Press2016.

[5] F. Mahdi, A. Hassanpour, F. Muller, An investigation on the evolution of granule formation by in-process sampling of a high shear granulator, Chemical Engineering Research and Design, 129 (2018) 403-411.

[6] J.S. Fu, Y.S. Cheong, G.K. Reynolds, M.J. Adams, A.D. Salman, M.J. Hounslow, An experimental study of the variability in the properties and quality of wet granules, Powder Technology, 140 (2004) 209-216.

[7] E.L. Chan, G.K. Reynolds, B. Gururajan, M.J. Hounslow, A.D. Salman, Blade–granule bed stress in a cylindrical high shear granulator: I—Online measurement and characterisation, Chemical Engineering Science, 86 (2013) 38-49.

[8] P.K. Le, P. Avontuur, M.J. Hounslow, A.D. Salman, A microscopic study of granulation mechanisms and their effect on granule properties, Powder Technology, 206 (2011) 18-24.

[9] A.M. Nilpawar, G.K. Reynolds, A.D. Salman, M.J. Hounslow, Surface velocity measurement in a high shear mixer, Chemical Engineering Science, 61 (2006) 4172-4178.

[10] V. Chouk, G. Reynolds, M. Hounslow, A. Salman, Single drop behaviour in a high shear granulator, Powder Technology, 189 (2009) 357-364.

[11] A.C. Scott, M.J. Hounslow, T. Instone, Direct evidence of heterogeneity during high-shear granulation, Powder Technology, 113 (2000) 205-213.

[12] J. Kristensen, V.W. Hansen, Wet granulation in rotary processor and fluid bed: Comparison of granule and tablet properties, AAPS PharmSciTech, 7 (2006) E153-E162.

[13] T.M. Chitu, D. Oulahna, M. Hemati, Wet granulation in laboratory-scale high shear mixers: Effect of chopper presence, design and impeller speed, Powder Technology, 206 (2011) 34-43.

[14] M. Ryan Fei Tzhung, C. Selomulya, K. Hapgood, Improved control of granule properties via "steady state" granulation, Chemeca 2013 (41st : 2013 : Brisbane, Qld.), Engineers Australia, Monash University, Victoria, 2013, pp. 611-616.

[15] K.J. Woyna-Orlewicz, R.;, Analysis of wet granulation process with plackett-burman design- case study, Acta Pol Pharm, 68 (2011) 9.

[16] N. Rahmanian, M. Ghadiri, X. Jia, Seeded granulation, 9th International Symposium on Agglomeration and 4th International Granulation Workshop, 2009, 206 (2011) 53-62.

[17] N. Rahmanian, M. Ghadiri, Y. Ding, Effect of scale of operation on granule strength in high shear granulators, Chemical Engineering Science, 63 (2008) 915-923.

[18] N. Rahmanian, A. Naji, M. Ghadiri, Effects of process parameters on granules properties produced in a high shear granulator, Special Issue on Agglomeration, 89 (2011) 512-518.

[19] S.J. Antony, M. Al-Sharabi, N. Rahmanian, T. Barakat, Shear stress distribution within narrowly constrained structured grains and granulated powder beds, Advanced Powder Technology, 26 (2015) 1702-1711.

[20] N.H. Rahmanian, M.H.; Kongb, C.C.; Patela, R.; Yusupb, S.; Mujtaba, I.M.;, An Experimental Investigation on Seeded Granulation of Detergent Powders, Chemical Engineering Transactions, 52 (2016) 6.

[21] A. Eliassi, H. Modarres, G.A. Mansoori, Densities of polyethyleneglycol and water mixtures in the 298.15–328.15 K temperature range, J. Chem. Eng. Data, 43 (1998) 719-721.
[22] P. Pandey, S. Badawy, A quality by design approach to scale-up of high-shear wet granulation process, Drug Development and Industrial Pharmacy, 42 (2016) 175-189.
[23] N. Rahmanian, T.E. Ganimi, M. Ghadiri, Further investigations on the influence of scale-up of a high shear granulator on the granule properties, Particuology, 11 (2013) 627-635.
[24] N. Rahmanian, M. Ghadiri, Strength and structure of granules produced in continuous granulators, Powder Technology, 233 (2013) 227-233.
[25] H.G. Merkus, Particle Size Measurements: Fundamentals, Practice, Quality (Particle Technology Series), Springer2009.
[26] T. Allen, Particle size measurement, Chapman & Hall, London, 1997.
[27] H.J. Ryu, F. Saito, Single particle crushing of nonmetallic inorganic brittle materials, Solid State Ionics, 47 (1991) 35-50.
[28] S. Antonyuk, J. Tomas, S. Heinrich, L. Mörl, Breakage behaviour of spherical granulates by compression, Chemical Engineering Science, 60 (2005) 4031-4044.
[29] A. Hassanpour, S. Joseph Antony, M. Ghadiri, Influence of interface energy of primary particles on the deformation and breakage behaviour of agglomerates sheared in a powder bed, Chemical Engineering Science, 63 (2008) 5593-5599.
[30] J. Litster, B. Ennis, The Science and Engineering of Granulation Processes, Springer Netherlands2013.
[31] D.M. Newitt, J.M. Conway-jones, A contribution to the theory and practice of granulation, rans. Inst. Chem Eng., 36 (1958) 422-441.
[32] T. Schaefer, C. Mathiesen, Melt pelletization in a high shear mixer. VIII. Effects of binder viscosity, International Journal of Pharmaceutics, 139 (1996) 125-138.
[33] Y. Chen, Y. Zhao, H. Gao, J. Zheng, Liquid bridge force between two unequal-sized spheres or a sphere and a plane, Particuology, 9 (2011) 374-380.
[34] D. Shi, J.J. McCarthy, Numerical simulation of liquid transfer between particles, Powder Technology, 184 (2008) 64-75.
[35] V.P. Mehrotra, K.V.S. Sastry, Pendular bond strength between unequal-sized spherical particles, Powder Technology, 25 (1980) 203-214.
[36] K. Hotta, K. Takeda, K. Iinoya, The capillary binding force of a liquid bridge, Powder Technology, 10 (1974) 231-242.
[37] G. Lian, C. Thornton, M.J. Adams, A Theoretical Study of the Liquid Bridge Forces between Two Rigid Spherical Bodies, Journal of Colloid and Interface Science, 161 (1993) 138-147.
[38] A. Hassanpour, M. Pasha, L. Susana, N. Rahmanian, A.C. Santomaso, M. Ghadiri, Analysis of seeded granulation in high shear granulators by discrete element method, Powder Technology, 238 (2013) 50-55.
[39] J.-G. Rosenboom, S. Antonyuk, S. Heinrich, M. Kraft, Characterisation of lactose powder and granules for multivariate wet granulation modelling, Chemical Engineering Science, 123 (2015) 395-405.
[40] S. Antonyuk, M. Khanal, J. Tomas, S. Heinrich, L. Mörl, Impact breakage of spherical granules: Experimental study and DEM simulation, Particulate Processes A Special Issue of Chemical Engineering and Processing, 45 (2006) 838-856.
[41] N. Rahmanian, M. Ghadiri, X. Jia, F. Stepanek, Characterisation of granule structure and strength made in a high shear granulator, Powder Technology, 192 (2009) 184-194.

List of Table

List of Figure

sample Sieved) Measurement for produced granules; (b) strength of granules in 500-600 μm range (shaded zone in (a)).

Fig 8: Schematic of the main granulation process stages: A) primary material (Durcal 65); B) wet granulation process (10 %wt of 65 %wt PEG4000 mixed with 90 %wt Durcal65) and drying; C) dried granule/agglomerate ready for resin and polishing; D) Detail of a single noncore-shell granule (core-shell not observed); E) core-shell granule (single crystal) and F) core-shelled granule (multiple crystals)

Fig 9: Explanation for the mechanism of granule formation: route (A) involves interaction of similar sized particles with droplets and forms liquid saturated nuclei, route (B) small particles attached to a large particle by liquid bridges. Forces resulting from collisions detach surface bound particles with weaker liquid bridges, and these may subsequently reattach in places where stronger bridges can form (e.g. nearer the surface of the large particle), Route (C) large particles interact with similar sized droplets, and form porous nuclei.

Fig 10: The force of adhesion times $(R_S + R_L)/R_S$ (data from Fig 5 in [35]) as a function of the particle size ratio. The detachment force of between two particles increase when the size of the large particle increases. For $R_L \to \infty$, a small particle on a plane, the force is $\approx 50\%$ higher compared to the force between two equal sized small particles.

Fig 11: Planes cut/polishing of different depth for the same granule depends on the polishing depth, the relationship of core diameter (D_c) and shell distance (δ_s) to the granule diameter (d_p)

Fig 12: The effect of impeller tip speed and different fill ratio (0.25, 0.50 and 0.75 of the bowl volume) in both scales on (A) the core-shell fraction ($f_{cs} = 1 - f_{nc}$) and (B) the ratio of shell distance to the total granule diameter. The black colour represents scale

0.5 L; the red colour represents scale 1.9 L. The data relates to the granules of 500 to 600 μm

Fig 13: SEM images used to evaluate the core-shell fraction of granules (500-600 μm): (A) Example with a significant amount of well-formed core shell granules formed in the 1.00 L material (50% full) at 5.39 m/s and (B) an example of a sample with few core shell particles lower generated in the 0.125 L material (25% full) at 3.50 m/s. The detachment process (in route B) is not very active resulting in little redistribution of fines around larger particles. For instance the particle in the dotted circle clearly shows a large particle partially surrounded by fines.

Fig 14: The effect of scales (0.5 and 1.9 L), impeller tip speed (3.50, 4.13, 5.39 and 6.12 m/s) and batch size (0.125, 0.250, 0.375, 0.50, 1.00 and 1.50 L) on the granules crushing strength for granules (500-600 μm). The patterned columns represent the average crushing strength of the 30 granules, with the error bars represent the standard deviations. For comparison, the dashed line shows the mean crushing strength of 8 MPa obtained by Rahmanian et al. [24] at 1L scale.

Table 1 The properties of the materials

Properties	Calcium carbonate (Durcal 65)	PEG 4000
Density (kg/m^3)	2745	1123
D10, D50 and D90 (μm) [1]	10.9, 64.9 and 254.9	----
Aspect Ratio Mean[1]	0.688	0.702
BET Surface Area, m^2/g	0.2877	----
Melting Point (°C)[2]	825	50-55
Initial pH	10.45	7.4
Solubility in water (%wt)[2]	0.0013	66
Circularity (d_{50})[1]	0.869	0.864

1-Using Malvern Morphology G3S, based on Volume
2-Melting points and Solubility in water were found from the MSDS sheet of the materials

Table 2 The amounts of materials charged and the operating conditions in each scale of granulator. The recipe charged is the same for all experiments

Scale (L)		**0.5**			**1.9**		
Batch volume (L)		0.125	0.250	0.375	0.500	0.100	1.500
Mass of Durcal 65 (g)		87.5	175	262.5	350	700	1050
Mass of PEG4000 (g)		9.7	19.5	29.5	39	78	117
Granulation Process	Speed (m/s)	3.50, 4.13, 5.39 and 6.12 where used with each fill ratio					
	Speed (rpm)	702, 806, 1053 and 1193			452, 533, 696 and 790		
	Time (s)	36	71	107	62	123	185

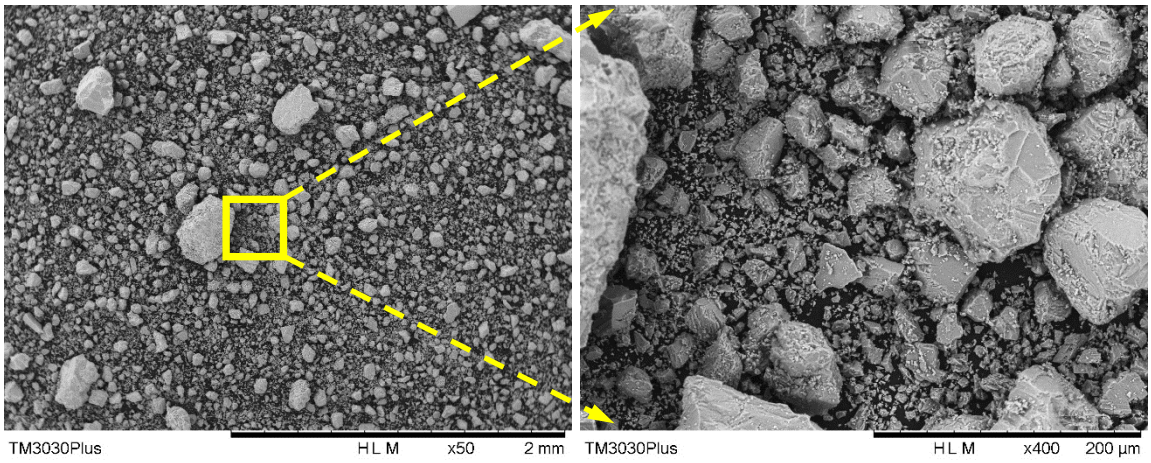

Fig 1 The morphology of calcium carbonate (Durcal 65)

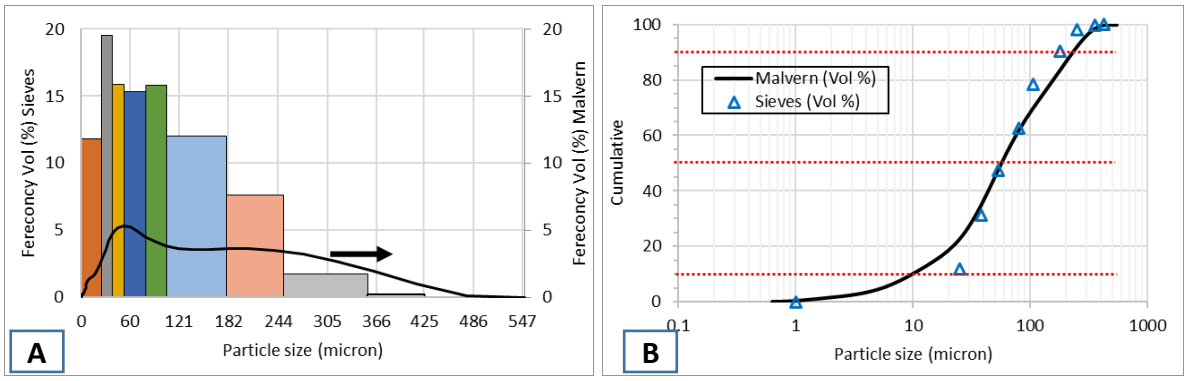

Fig 2 Calcium carbonate (Durcal 65) particle size distribution: Sieves (different colours represent different sieve mesh size) and Malvern 2000 analysis.

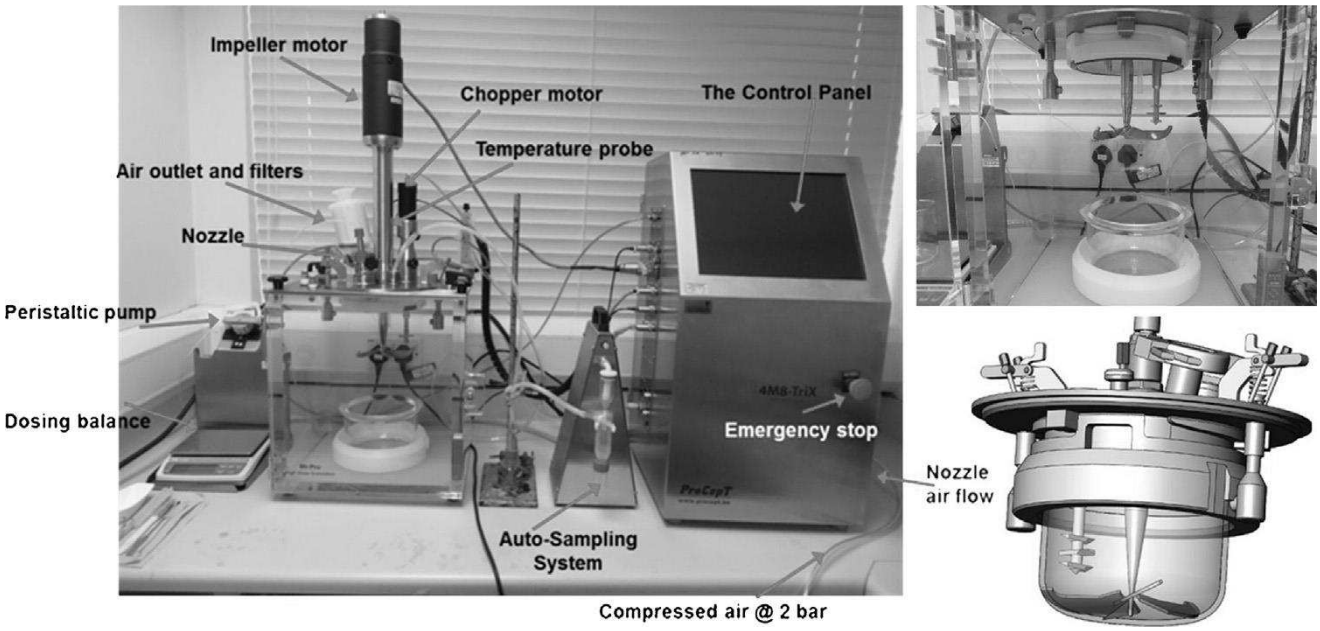

Fig 3 Mi-Pro - High Shear Wet-Granulator – ProCepT

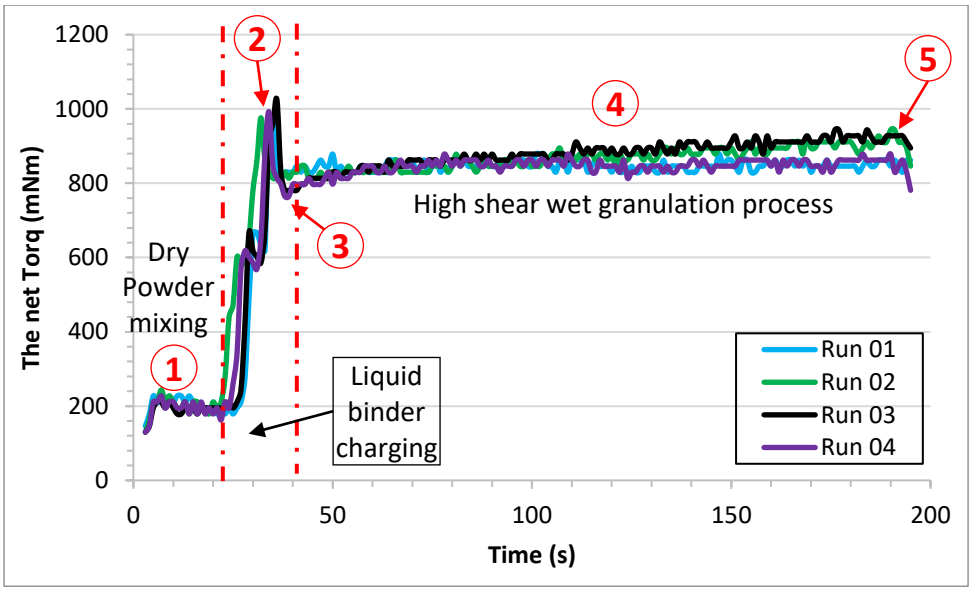

Fig 4 Three values of the net torque based on the stages of granulation process for 1.5 L feed volume using large scale (1.9L) at impeller tip speed of 4.12 m/s. Stage (1) shows the net torque for the mixing of solid particles without any liquid. Stages (2) and (3) show the maximum and minimum net torque respectively after adding the liquid binder. Stages (4) and (5) show the average and the maximum net torque, respectively once the binder is well distributed

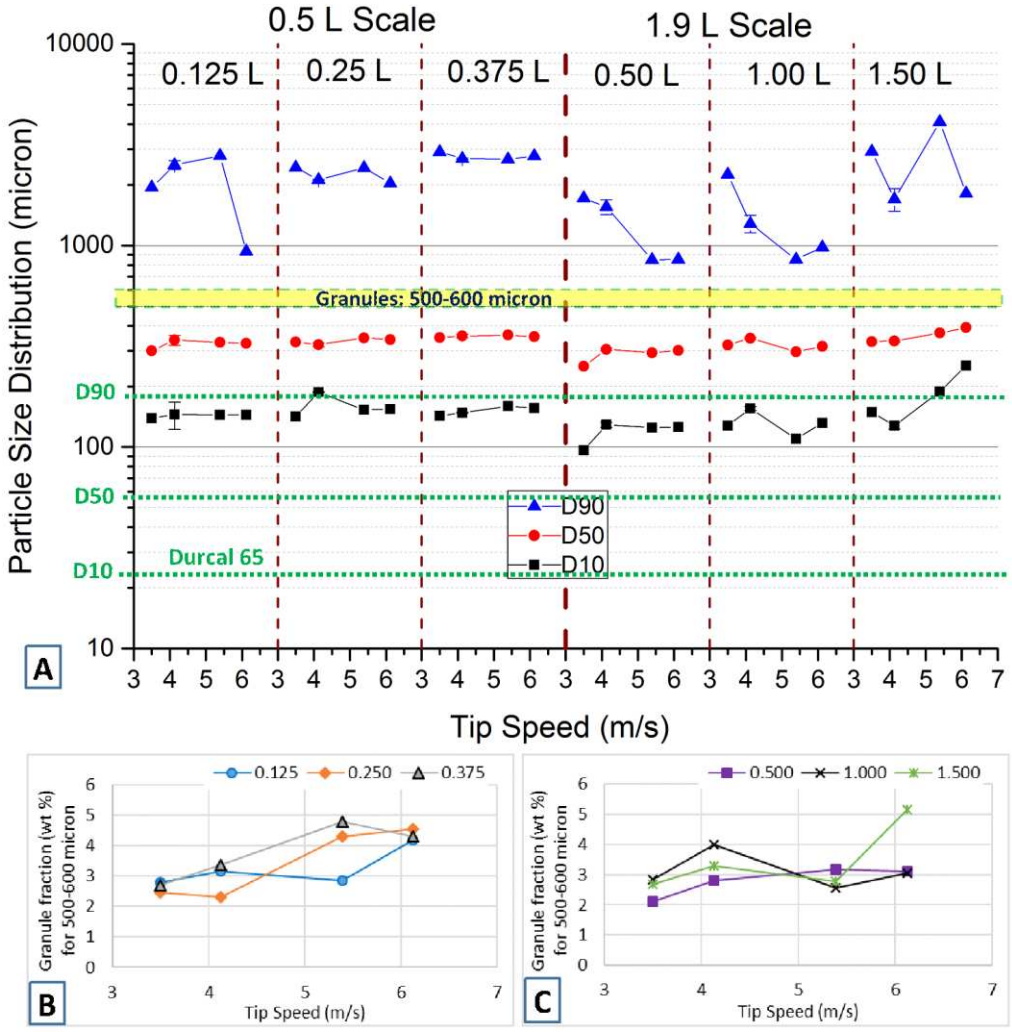

Fig 5 A) Granules size distribution (D10, D50 and D90) based on sieves analysis for different batch volume at the four impeller tip speeds (3.50, 4.13, 5.39 and 6.12 m/s). Error bars, represent the standard deviations of four runs for each experiment at 4.13 m/s. The green detached lines show the D10=23, D50=58 and D90=180 of the initial material (calcium carbonate) and the yellow bar represents granules within the size of 500-600 μm that have been analysed and studied in this work. B) and C) are the granule fraction (wt%) for 500-600 micron using both scales (small and large respectively) and different conditions.

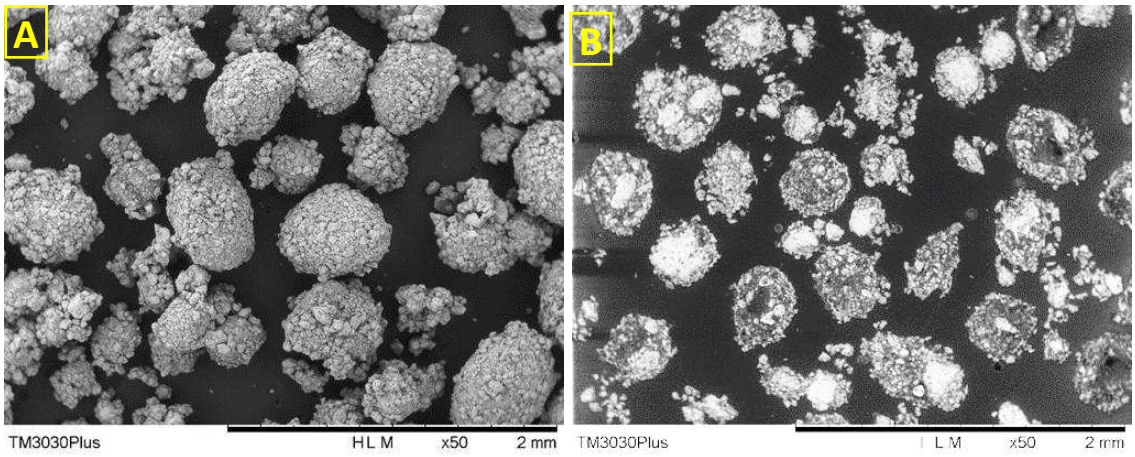

Fig 6 Typical SEM images of A) granules and B) polished slice in the size range of 500-600 μm

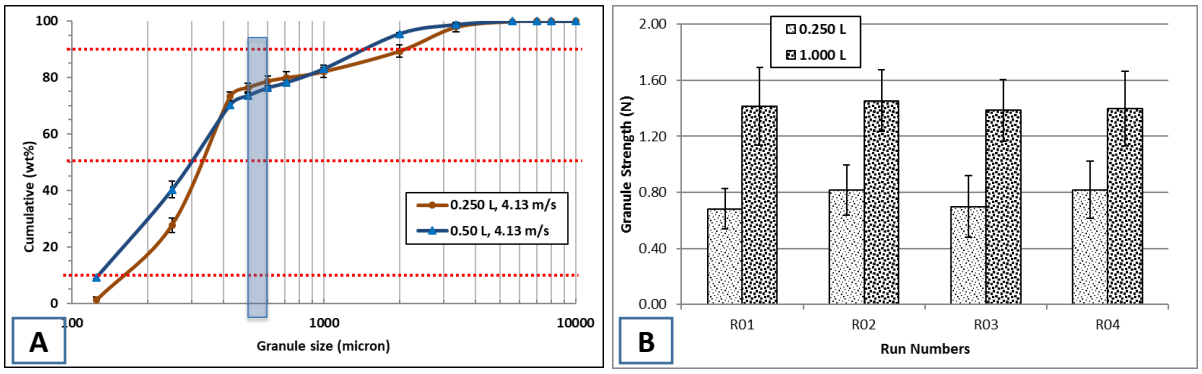

Fig 7 Reproducibility of granulation process using 0.25 L and 1.00 L within smaller (0.5 L) and larger (1.9 L) scales at constant impeller tip speed rule of 4.13 m/s: (A) PSD (full sample Sieved) Measurement for produced granules; (B) strength of granules in 500-600 μm range (shaded zone in (a))

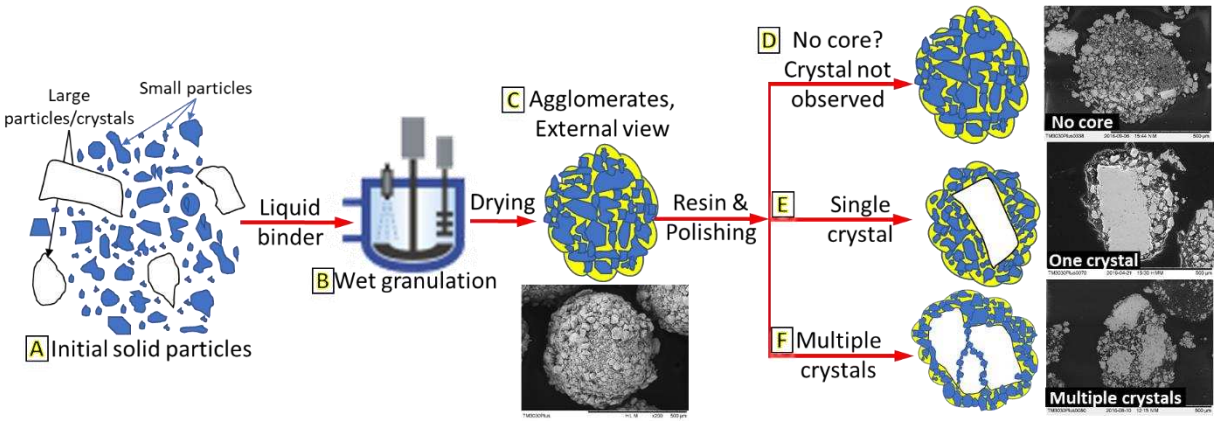

Fig 8 Schematic of the main granulation process stages: A) primary material (Durcal 65); B) wet granulation process (10 %wt of 65 %wt PEG4000 mixed with 90 %wt Durcal65) and drying; C) dried granule/agglomerate ready for resin and polishing; D) Detail of a single noncore-shell granule (core-shell not observed); E) core-shell granule (single crystal) and F) core-shelled granule (multiple crystals)

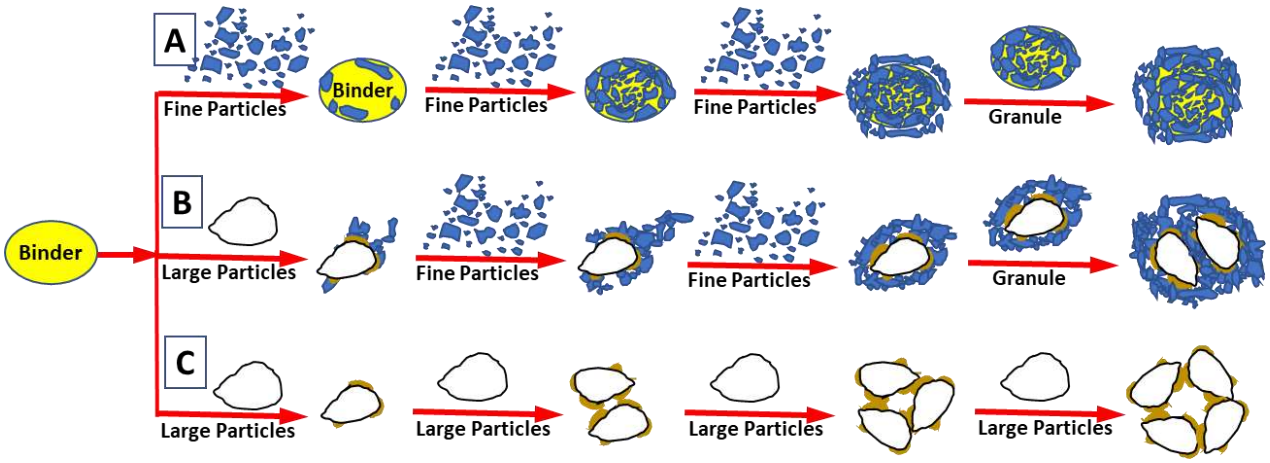

Fig 9 Explanation for the mechanism of granule formation: route (A) involves interaction of similar sized particles with droplets and forms liquid saturated nuclei, route (B) small particles attached to a large particle by liquid bridges. Forces resulting from collisions detach surface bound particles with weaker liquid bridges, and these may subsequently reattach in places where stronger bridges can form (e.g. nearer the surface of the large particle), Route (C) large particles interact with similar sized droplets, and form porous nuclei.

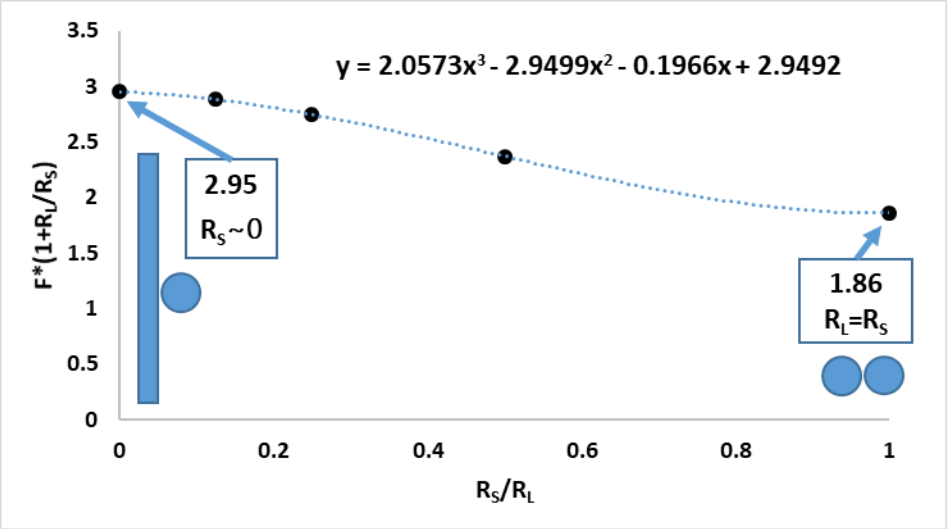

Fig 10 The force of adhesion times $(R_S + R_L)/R_S$ (data from Fig 5 in [35]) as a function of the particle size ratio. The detachment force of between two particles increase when the size of the large particle increases. For $R_L \to \infty$, a small particle on a plane, the force is $\approx 50\%$ higher compared to the force between two equal sized small particles.

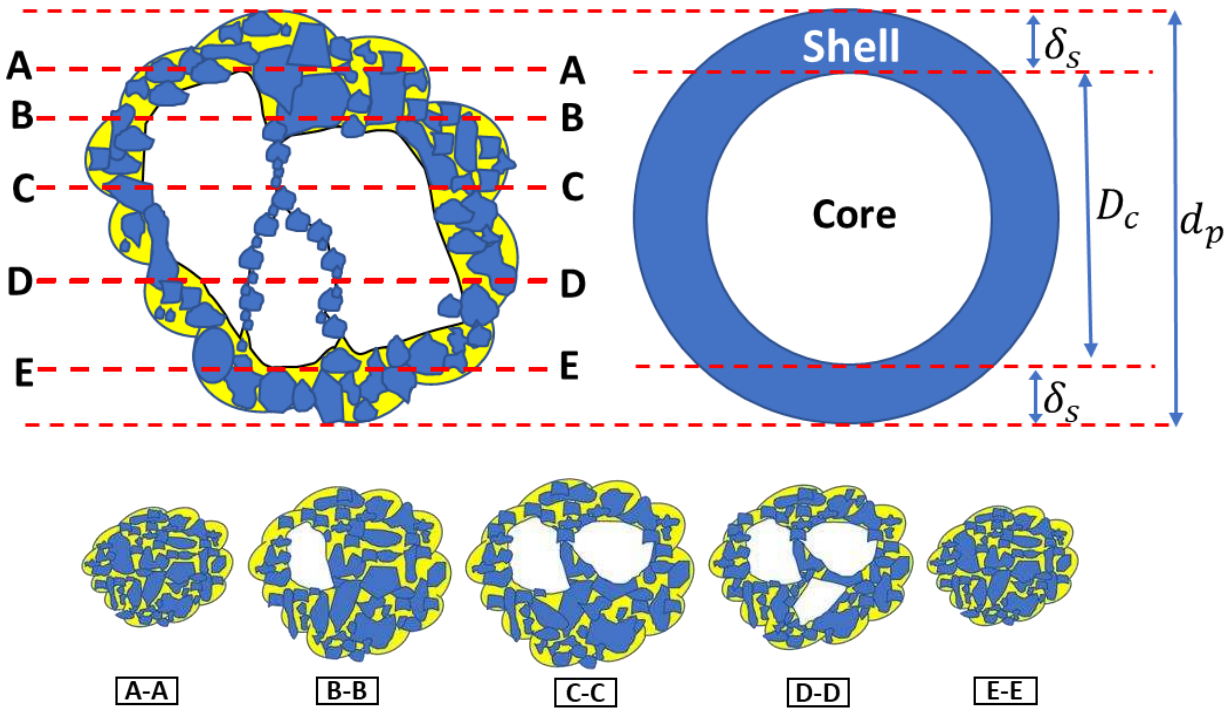

Fig 11 Planes cut/polishing of different depth for the same granule depends on the polishing depth, the relationship of core diameter (D_c) and shell distance (δ_s) to the granule diameter (d_p)

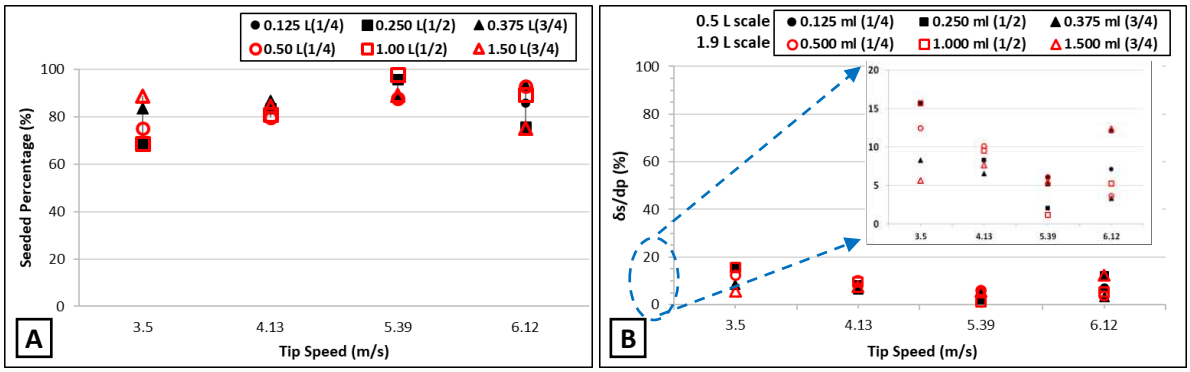

Fig 12 The effect of impeller tip speed and different fill ratio (0.25, 0.50 and 0.75 of the bowl volume) in both scales on (A) the core-shell fraction ($f_{cs} = 1 - f_{nc}$) and (B) the ratio of shell distance to the total granule diameter. The black colour represents scale 0.5 L; the red colour represents scale 1.9 L. The data relates to the granules of 500 to 600 μm.

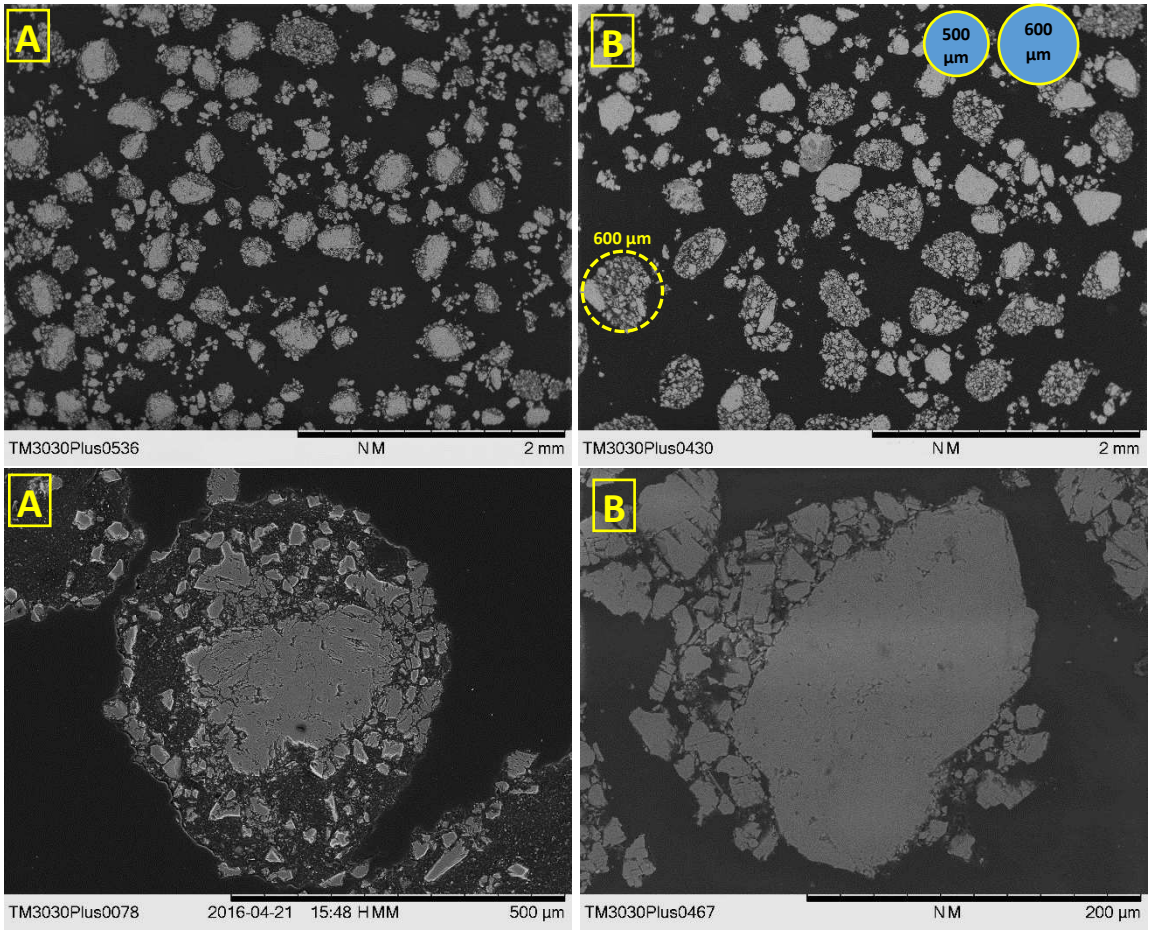

Fig 13 SEM images used to evaluate the core-shell fraction of granules (500-600 µm): (A) Example with a significant amount of well-formed core shell granules formed in the 1.00 L material (50% full) at 5.39 m/s and (B) an example of a sample with few core shell particles lower generated in the 0.125 L material (25% full) at 3.50 m/s. The detachment process (in route B) is not very active resulting in little redistribution of fines around larger particles. For instance the particle in the dotted circle clearly shows a large particle partially surrounded by fines.

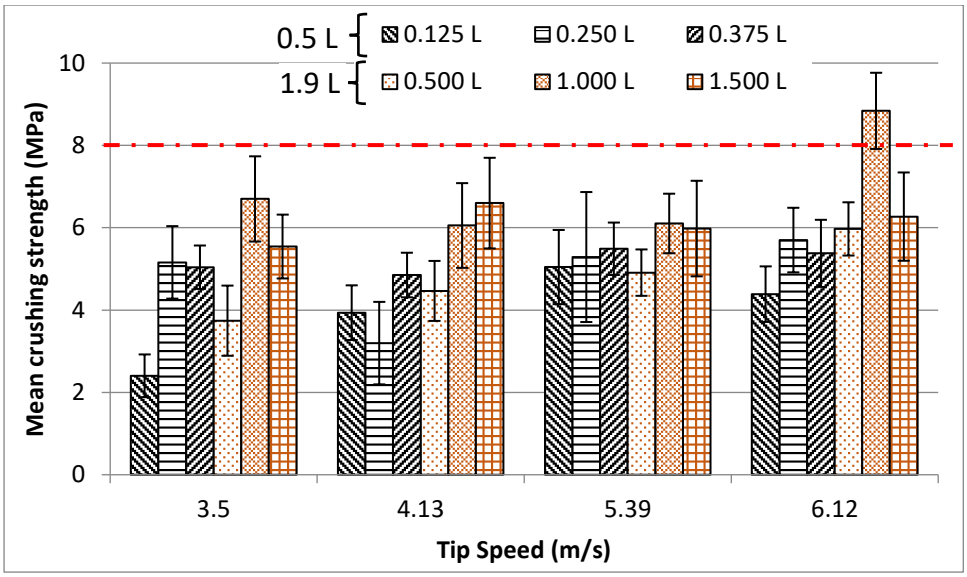

Fig 14 The effect of scales (0.5 and 1.9 L), impeller tip speed (3.50, 4.13, 5.39 and 6.12 m/s) and batch size (0.125, 0.250, 0.375, 0.50, 1.00 and 1.50 L) on the granules crushing strength for granules (500-600 μm). The patterned columns represent the average crushing strength of the 30 granules, with the error bars represent the standard deviations. For comparison, the dashed line shows the mean crushing strength of 8 MPa obtained by Rahmanian et al. [24] at 1L scale.